ACS Photonics

Article

pubs.acs.org/journal/apchd5

Ultrafast Photoluminescence in Quantum-Confined Silicon Nanocrystals Arises from an Amorphous Surface Layer

Daniel C. Hannah,[†] Jihua Yang,[‡] Nicolaas J. Kramer,[‡] George C. Schatz,[†] Uwe R. Kortshagen,[‡] and Richard D. Schaller*[,†,§]

[†]Department of Chemistry, Northwestern University, Evanston Illinois 60208, United States

[‡]Department of Mechanical Engineering, University of Minnesota, 111 Church Street Southeast, Minneapolis, Minnesota 55455, United States

[§]Center for Nanoscale Materials, Argonne National Laboratory, Argonne, Illinois 60439, United States

Supporting Information

ABSTRACT: Here, we examine ultrafast photoluminescence produced from plasma-grown, colloidal silicon nanocrystals as a function of both particle size and lattice crystallinity. In particular, we quantify the decay time and spectral profiles of nominally few-picosecond direct-gap emission previously attributed to phononless electron−hole recombination. We find that the high-energy (400−600 nm, 2−3 eV) photoluminescence component consists of two decay processes with distinct time scales. The fastest photoluminescence exhibits an ∼30 ps decay constant largely independent of emission energy and particle size. Importantly, nearly identical temporal components and blue spectral features appear for amorphous particles. We thus associate high-energy, rapid emission with an amorphous component in all measured samples, as supported by Raman analysis and molecular dynamics simulation. Based on these observations, we advise that the observed dynamics proceed too slowly to originate from intraband carrier thermalization and instead suggest a nonradiative origin associated with the amorphous component.

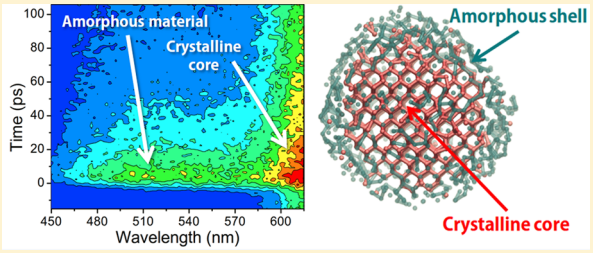

KEYWORDS: *quantum dot, nanocrystal, photoluminescence, silicon, amorphous silicon, spectroscopy*

Nanosized forms of silicon such as quantum-confined, colloidally prepared nanoparticles (NPs) have been the subject of significant attention owing to widely tunable, bright photoluminescence (PL) and the possibility that particle size reduction in the material may yield phononless, direct gap optical transitions.[1−4] Whereas bulk Si radiates with negligible efficiency owing to an indirect-gap lowest-energy interband transition, nanosized Si often exhibits 10% or greater quantum yield with reported decay components spanning microsecond to picosecond time scales.[2,5−13] However, despite numerous studies, disagreement exists regarding the origin of both the fast and slow decay processes. For instance, a 650−1000 nm PL feature (termed throughout this manuscript as the "red" feature) that displays a microsecond lifetime is commonly attributed either to slow emission arising from surface-localized radiative traps[6,9,13,14] or to radiative recombination from NP core states exhibiting indirect character.[5,15−18] In this work, however, we focus on characterization of the radiative recombination that occurs in the 400 to 600 nm energy range, referred to herein as the "blue" feature.

Significant excitement exists with regard to multiple reports of fast (nanosecond to subnanosecond) 400 to 600 nm (2−3 eV) PL decay features in Si NPs.[2,5,13,19,20] Observations of such blue emission, which appear for both Si NPs produced via wet chemical synthesis[21,22] as well as for plasma-grown materials,[2] are often attributed to emergent direct gap optical transitions[2,5,20] that may arise from at least two possible mechanisms. First, the bulk semiconductor requirement of carrier energy and linear momentum conservation can become less stringent upon quantum-confinement owing to replacement of electronic band structure with discrete electronic states, in similarity to molecules.[23,24] In addition, during the time that a photoexcited electron and hole (an exciton) collectively exceed the lowest energy "band-edge" transitions (∼1 ps in most semiconductor nanomaterial compositions),[25,26] radiative recombination can occur between states that possess the same momentum and do not necessitate involvement of a momentum-conserving phonon.[5] Observation of such "phononless" emission from hot exciton states requires either large oscillator strength or slowed cooling of hot excitons.

A recent report utilized time-resolved PL spectroscopy and a quasi-continuous sample re-excitation scheme in order to accentuate and spectrally characterize blue emission features, but lacked sufficient time-resolution to directly characterize the time scale of the recombination process.[5] An additional study also suggested that direct-gap transitions my arise in colloidally prepared, alkyl-terminated NPs owing to modification of the

Received: April 30, 2014
Published: September 8, 2014

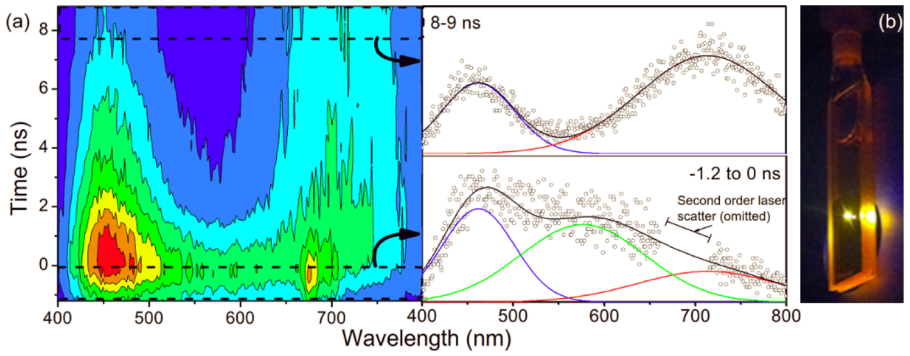

Figure 1. (a) A streak camera image for crystalline 3.2 nm diameter Si NPs photoexcited at 325 nm (3.8 eV). Dynamics over a 10 ns time window subsequent to photoexcitation are shown. The apparent buildup of PL prior to $t = 0$ is related to an instrumentally limited response. The panels on the right side show PL spectra integrated temporally over the regions indicated by the dotted lines and arrows in the left panel (top right panel: PL spectra from 9−10 ns, bottom right panel: 0−1 ns). Solid lines in the right panels indicate Gaussian lineshapes used to fit the PL spectra. The peak centers and line widths obtained from the fits in the 9−10 ns spectra were fixed and used in the fitting of the 0−1 ns spectra, a procedure justified by the absence of temporal evolution in the PL line width. In the bottom right panel, data points from 650−700 nm are contaminated by second order scatter from the 325 nm excitation source; these points are omitted from the plot and the Gaussian fitting procedure. (b) A photo showing PL from 3.2 nm diameter Si NPs.

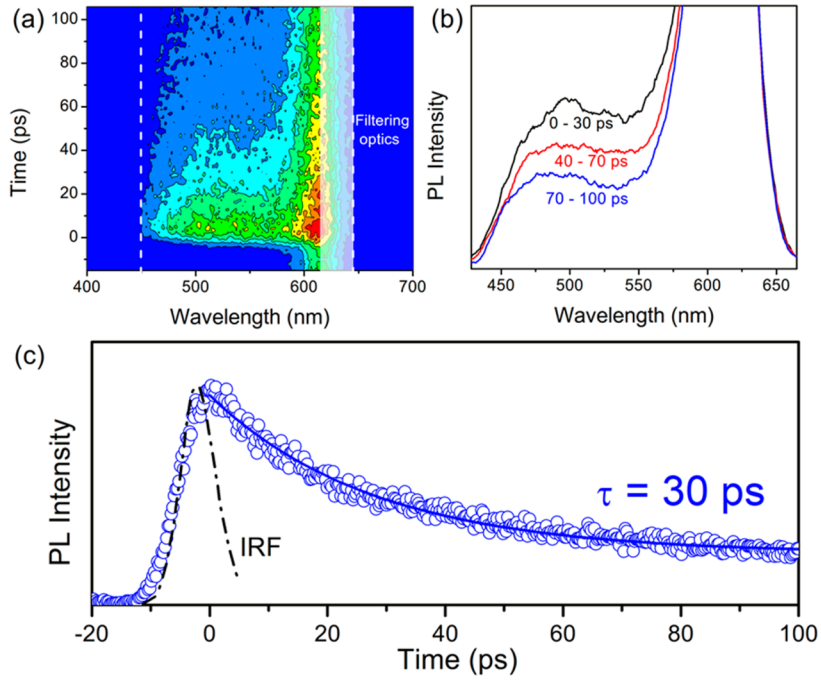

Figure 2. (a) Streak camera image of PL from the 3.2 nm diameter Si NPs recorded for 100 ps following photoexcitation. Necessary filtering optics and sample reabsorptions artificially truncate the PL spectrum on the red and blue edges. Truncation due to band-pass filtering is indicated by dashed white lines, while the translucent white shading indicates regions where signal is attenuated by the filtering optics, but not completely blocked. The high-energy tail of the red PL band is apparent as a long-lived shelf, as it does not fully relax prior to re-streaking of the time-resolving detector. (b) Main panel: Time-resolved PL spectra in three different temporal regions for the same sample. Temporally binned regions are indicated by labels. (c) Time-resolved PL dynamics spectrally integrated from 475 to 525 nm. The solid blue line indicates a fit of the dynamics to a single exponential decay function. The instrument response function (IRF) is indicated by a dotted black line. Note that this IRF corresponds only to a streak camera observation window of 120 ps (see Methods section for details).

electronic structure by covalent surface functionalization.[13] In this case, 400−600 nm emission does not compete with intraband relaxation, but instead, hybridization with the covalently attached surface ligands purportedly modifies the band-edge electronic wave functions such that substantial broadening of the related *k*-space distribution occurs, permitting direct recombination at the Γ-point. That report concludes that high-energy emission stems from recombination produced within the Si NPs rather than from defect states, but the dynamics of the obtained PL spectra were not characterized with sufficient time-resolution to distinguish processes related to carrier thermalization.

Here, we examine multiple sizes and degrees of crystallinity of plasma-synthesized colloidal Si NPs using a previously reported synthetic method[27] with a focus on emission in the 400−600 nm "blue" spectral region. We spectrally and, for the first time, temporally resolve PL from the particles with up to single-picosecond time resolution. From these measurements we observe a ∼30 ps decay component as the fastest PL relaxation time scale. This spectral and temporal resolution

dx.doi.org/10.1021/ph500145p | *ACS Photonics* 2014, 1, 960−967

allows us to definitively assign lifetimes to the observed PL features. Based on our observations, we suggest that the blue PL band in Si NPs originates from an amorphous component in the samples and that the rapid emission processes are too slow to be consistent with a hot exciton radiative process. We also show through molecular dynamics (MD) simulations that experimental Raman spectra obtained at different plasma powers are well-described by particles presenting a thin, amorphous surface (consistent with electron microscopy) which we suggest gives rise to the fast emission.

RESULTS

Ultrafast PL Dynamics of Highly Crystalline Silicon (c-Si) Nanoparticles. Crystalline Si-NPs were synthesized in a radio frequency (RF) plasma (80 W) and covalently functionalized with 1-dodecane using the methods described below (see Methods). Single-exciton PL dynamics under ambient conditions were examined using a streak camera, which provides simultaneous spectral and temporal resolution (see Methods). Figure 1 (left panel) depicts a streak camera image of PL recorded for the first 10 ns following photoexcitation of an ensemble of 3.2 nm-diameter crystalline Si (c-Si) NPs. The top right panel of Figure 1 shows a late-time PL spectrum (temporally integrated from 9−10 ns), which reveals two clear contributions: a blue PL band centered near 450 nm and a red PL band centered at 700 nm. The presence of distinct blue and red bands is consistent with many previous reports,[2,19−22] although their origins remain disputed. PL immediately following the excitation pulse (integrated from 0−1 ns, shown in the bottom right panel of Figure 1) reveals a third PL band intermediate in energy, termed the "green" feature. Such a green feature was reported by de Boer et al., who attributed it to phononless radiative recombination of hot excitons, despite a lack of direct dynamical characterization.[5]

To investigate the fast dynamics of these features we examined PL using single-picosecond temporal resolution streak camera electronics. Such high time resolution measurements applied to a broadband emitter necessitate the use of bandpass spectral filtering in order to obtain wavelength-resolved dynamics free from artifacts. Figure 2a depicts a streak camera image of PL from the same ensemble of 3.2 nm diameter c-Si NPs for 100 ps following photoexcitation. Because of required filtering optics, only the high-energy shoulder of the red PL band is observed and the high-energy edge of the blue PL band is also truncated. Truncation due to filtering optics is indicated in Figure 2a. The red feature exhibits a microsecond decay lifetime and is present in this data as a persistent shelf. The blue feature, however, exhibits decay on this time scale; this is evident in the time-resolved spectra displayed in Figure 2b for the same sample. Notably, aside from decreasing intensity with time, the spectra exhibited little temporal evolution in terms of both energy and spectral profile. For all c-Si NP sizes studied, the PL spectral profile remains relatively constant for 800 ps following photoexcitation. Notably, the consistent PL profile at blue wavelengths suggests that the decay in PL intensity is due to the collective depletion of a single population of emitters. We explore the blue feature dynamics further in Figure 2c, which displays PL intensity at 500 nm as a function of time for the same sample. Comparison to the instrument response function (IRF, also shown in Figure 2c) obtained from examination of pump laser scatter indicates that the blue feature decay is well-resolved at these time scales and that no faster dynamics are taking place in the system with significant amplitude. Fitting the dynamics in Figure 2c to a monoexponential decay function yields a time constant of 28 ps. At slightly longer times, a subnanosecond decay component is also observed. Fitting the dynamics from 0 to 800 ps to a biexponential decay function yields time constants corresponding to the ∼30 ps feature discussed above and a component having a lifetime that is consistently hundreds of picoseconds (see Table 1 for fitting results and Supporting Information for PL dynamics from 0−800 ps).

Table 1. Time Constants for the Biexponential Decay Observed in the PL Dynamics for the First 800 ps Following Photoexcitation of 4 Silicon NP Sizes[a]

c-Si NP diameter (nm)	τ_1 (ps)	τ_2 (ps)
2.6	27.8 ± 0.6	204 ± 7
3.2	26 ± 4	243 ± 12
3.8	16 ± 1	195 ± 13
4.6	26 ± 7	563 ± 47

[a]Errors are derived from the fitting function.

Notably, picosecond scale dynamics do not reveal distinct blue and green decay components, indicating that the green feature noted in Figure 1 displays dynamics that are indistinguishable from the blue feature on picosecond time scales, and that no spectral range exhibits decay dynamics having a time constant faster than ∼20 ps.

Characterization of Amorphous Silicon Nanoparticles. In addition to highly crystalline particles, we examined reduced crystallinity Si NPs produced using lower plasma power as described and characterized in depth in recent reports.[27,28] Noting numerous reports of visible PL from amorphous silicon structures,[29−31] we systematically investigated the role of lattice crystallinity on PL spectrum. Figure 3a depicts Raman scattering collected from Si NPs synthesized at plasma powers of 8, 30, 45, and 60 W. NPs synthesized at higher powers clearly yield more narrow Raman scattering spectra, consistent with higher crystallinity samples. The NPs synthesized at 8 W exhibit a broad, featureless peak, corresponding to an entirely amorphous sample.[27] We also present the Raman scattering spectrum of bulk crystalline Si, which exhibits a sharp peak at 520 cm^{-1} corresponding to the transverse optical (TO) phonon mode. This peak is also clearly present in the Si NP Raman scattering spectra, along with a low-frequency shoulder, the presence of which has been correlated with amorphous materials.[32] The relative intensity of the low-frequency shoulder appears to be larger for lower plasma powers.

To gain a clearer understanding of the correspondence between Raman spectra, sample crystallinity, and address the potential coexistence of crystalline and amorphous phases, we performed MD simulations of experimentally sized (4 nm diameter) Si NPs that present varying amounts of amorphous material on the surface. The construction of particles presenting an amorphous surface was motivated by the clear presence of a disordered surface layer in transmission electron microscopy (TEM) images of Si NPs in addition to the presence of stretching modes in the infrared absorption spectrum (see Supporting Information), which are attributed to under-coordinated Si species (SiH_2 and SiH_3). Using force constants obtained from a relaxation of interatomic forces in the structures, we computed expected Raman scattering spectra. The details of amorphous structure generation, molecular dynamics simulations, and Raman scattering calculations can be

dx.doi.org/10.1021/ph500145p | ACS Photonics 2014, 1, 960−967

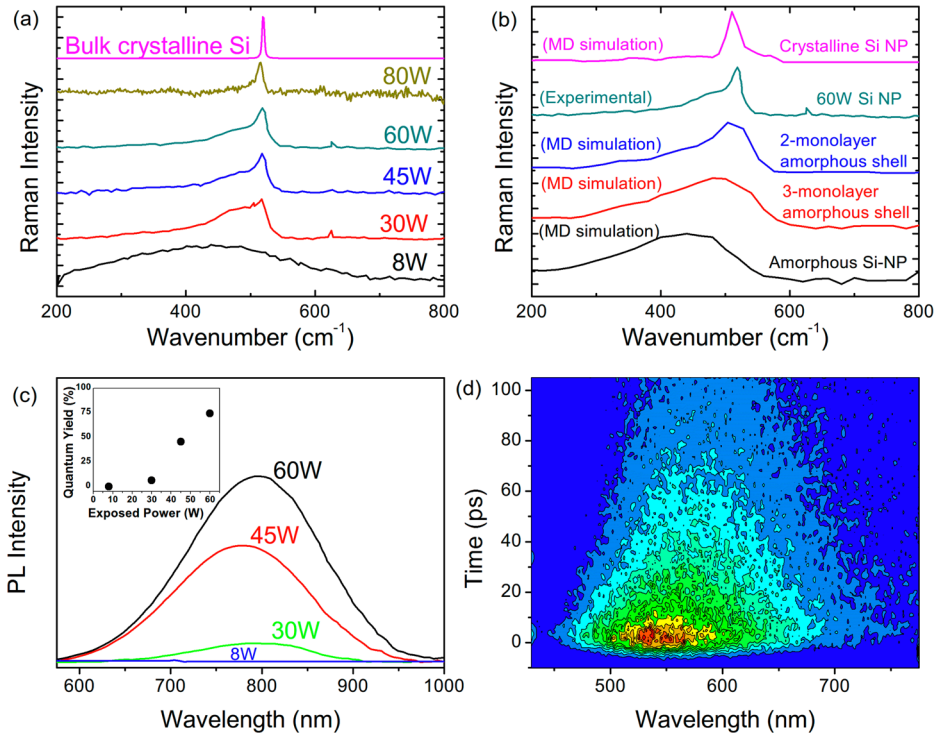

Figure 3. (a) Raman scattering spectrum of Si NPs synthesized at the indicated plasma powers. The peak at 500 cm^{-1} is attributed to the transverse optical (TO) phonon and diminishes in intensity for samples synthesized at lower powers (less crystalline). The Raman scattering spectrum of bulk crystalline Si is also displayed. All Raman spectra have been mathematically normalized and plotted with a vertical offset. (b) Raman scattering spectra for Si NPs predicted from MD simulations (see Supporting Information for computational methods). Color-coded data is shown for a fully crystalline particle, particles with 2 or 3 monolayers of amorphous Si on their surfaces, and a fully amorphous particle. The experimental data for Si NPs synthesized at 60 W from (a) is reproduced here for comparison. (c) PL spectra of Si NPs synthesized at four different plasma powers (indicated on the figure). Higher plasma powers nominally yield more crystalline samples. Inset: PL quantum yield for Si NPs as a function of the plasma power used during their synthesis. (d) A streak camera image of PL from Si NPs synthesized at a plasma power of 8 W (e.g., fully amorphous Si). Photoexcitation energy was 3.8 eV.

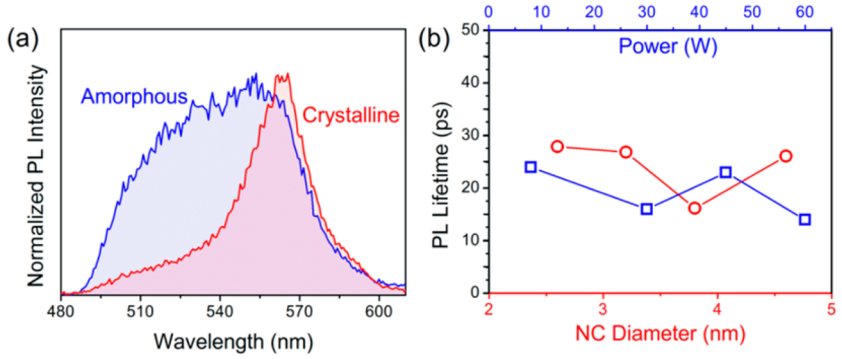

Figure 4. (a) Mathematically normalized PL spectra temporally binned from 0−100 ps following photoexcitation for Si NPs synthesized for amorphous (8 W) and crystalline (60 W) Si NPs, which are indicated on the figure. Although filtering optics artificially truncate the red edge of the PL spectrum, the same optics were used in collection of both PL spectra displayed. (b) Lifetime of the fastest dynamics observed for all of the samples considered in this study. The blue (squares) data and top axis correspond to the Si NPs synthesized at indicated plasma powers, while the red (circles) data and bottom axis correspond to four sizes of highly crystalline Si NPs.

found in the Supporting Information. Figure 3b displays the MD-derived Raman scattering spectra for four particles: A fully crystalline particle, particles with either 2 or 3 monolayers of amorphous material on the surface and an entirely amorphous particle. These simulations suggest that increasing amounts of amorphous material on crystalline core give rise to a lower-frequency shoulder near the TO feature. The experimental Raman scattering for Si NPs synthesized at 60 W (Figure 3a) is also reproduced on this graph for comparison. The calculated Raman spectrum of the entirely crystalline Si NP lacks good agreement with experimental data. Notably, however, the calculated Raman spectrum for a particle presenting a 2-monolayer amorphous Si shell closely replicates the experimental spectrum. Asymmetric broadening of the TO peak in the presence of amorphous material was previously reported by Duan et al. In analysis of Raman scattering from matrix-embedded Si nanocrystals, they attribute a similar low-frequency shoulder to amorphous material but do not comment further on the origin or character of such material.[32] Additionally, a comparison of TEM to Raman-based NP sizing

dx.doi.org/10.1021/ph500145p | ACS Photonics 2014, 1, 960−967

methods lead Ristić and co-workers to suggest that a shell of amorphous material could explain the observed discrepancies in the NP sizes obtained.[33] The persistence of a disordered surface, even in the absence of organic ligands, led to a similar suggestion by Panthani et al.[34] The Raman spectrum of nanocrystalline Si, in conjunction with the Raman spectrum of purely amorphous Si, can be used to estimate the relative amounts of amorphous and crystalline material.[35] In brief, the ratio of crystalline and amorphous TO phonon peak areas, with appropriate scaling, reflects the fraction of crystalline material in the sample. By applying the method put forth in ref 35 to our Si NPs, we find that the 8, 30, 45, 60, and 80 W samples contain 100, 62, 57, 48, and 35% of entirely amorphous material, respectively (see Supporting Information for fitting procedure details).

The static PL spectra of the Si NPs studied here are dominated by broad emission corresponding to the red (indirect-gap) PL band for all plasma-synthesis powers, as shown in Figure 3c. Quantum yield clearly increases with increasing plasma powers (Figure 3c, inset). Figure 3d depicts a streak camera image of PL from an ensemble of Si NPs synthesized at 8 W (least crystalline) for 100 ps following photoexcitation. A single strong emission band is evident, centered roughly at 550 nm. Comparisons of the PL decay shown in Figure 3c to the PL rise and IRF indicates that these dynamics are well-resolved and that no faster processes occur.

Next, we compare c-Si NPs and amorphous silicon nanoparticles (a-Si NPs). The spectral profile of the initial PL amplitude (integrated temporally from 0−100 ps following photoexcitation) for 4 nm diameter a-Si NPs shows a systematic dependence on plasma power, as depicted in Figure 4a. Figure 4a shows normalized PL spectra temporally integrated from 0−100 ps for our most and least crystalline samples. a-Si NPs produced using low power (8 W) show a broad PL band centered at ∼550 nm. The Si NPs made at higher plasma power (60 W) continue to produce blue PL but also exhibit increased red PL intensity, the high energy shoulder of which is evident in Figure 4a (required filtering optics truncate the majority of the red emission band, as indicated in Figure 2a). Given that all four samples exhibit similar size and organic ligand termination, the data in Figure 4a, which have been normalized for comparison of spectral profiles, strongly suggest that the observed differences in PL spectra are related to the extent of Si NP crystallinity. In light of this, we attribute blue-feature PL to emission from remnant amorphous material in the Si NP ensemble, which we suggest is present as a shell of amorphous material. With higher plasma power, the relative amount of amorphous material decreases as more crystalline NPs are produced (Figure 3b), whereupon long-lived, indirect-gap excitonic (red-feature) PL dominates the emission spectrum (Figure 4a) at every time range.

DISCUSSION

We aim to resolve the origin of blue PL photons emitted from Si NPs as well as the processes responsible for the decay of the associated PL band (the blue feature). Regarding the dynamics of the blue PL feature, we note that the NP size-independent fastest PL decay of ∼30 ps is an order of magnitude slower than typical intraband relaxation time in quantum-confined materials,[25,26] a process with which phononless PL would be competitive. Conversely, if indeed the rapid PL decay were associated with hot carrier recombination, it would imply the slowest intraband relaxation time ever reported for core-only colloidal NPs. Furthermore, the red PL feature, which we recently established arises from lowest-energy exciton states within the NP core,[15] does not exhibit a rise time that correlates with the "green" feature decay (as observable at 525 nm in Figure 2a), consistent with ultrafast (1 ps or less) relaxation of hot excitons as found in numerous other semiconductor NPs.[25,26] This lack of a correlated rise time offers additional evidence that the ∼30 ps decay does not represent a hot exciton radiative process.

Instead, we posit that the ∼30 ps decay feature arises from a nonradiative process associated with amorphous material. Indeed, if a radiative process were responsible, the biexponential dynamics would imply two separate populations of emitters with different associated PL line widths. Given the unchanging PL profile (Figure 2b), it is unlikely that biexponential dynamics arise from two separate radiating populations. This notion is further supported by the absence of a strong optical absorption transition in this spectral region.[36] Considering the oscillator strength, which would be associated with such a rapid radiative transition, it is highly unlikely that a 30 ps decay (which represents the upper bound of our lifetime measurements) caused by optical transitions would have no apparent manifestation in the optical absorption spectrum of the Si NPs. Fermi's Golden Rule allows us to relate the optical radiative rate (τ_{PL}^{-1}) to the optical transition matrix element $|\langle\psi_1|\hat{p}|\psi_0\rangle|^2$ via eq 1:

$$\tau_{PL}^{-1} = \frac{e^2 n\omega}{\pi\varepsilon_0 m^2 \hbar c^3} |\langle\psi_1|\hat{p}|\psi_0\rangle|^2 \quad (1)$$

In eq 1, e is the fundamental charge, n is the refractive index of silicon, $\hbar\omega$ is the emission energy, ε_0 is the vacuum permittivity, m is the electron mass, and c is the speed of light in vacuum. Coupled with the expression for oscillator strength ($f = (2/\hbar m\omega)|\langle\psi_1|\hat{p}|\psi_0\rangle|^2$), we can express the oscillator strength of a given equation in terms of its radiative lifetime, as shown in eq 2:

$$f = \frac{2\pi\varepsilon_0 mc^3}{e^2 n\omega^2} \frac{1}{\tau_{PL}} \quad (2)$$

For the 30 ps decay ($\hbar\omega$ = 2.75 eV, τ_{PL} = 30 ps), a radiative transition would be associated with an oscillator strength of f = 13.8. By comparison, the long-lived red PL ($\hbar\omega$ = 1.75 eV, τ_{PL} = 75 μs) has an oscillator strength of $f = 1.3 \times 10^{-5}$, which is several orders of magnitude smaller. Provided that significant silicon atom rearrangements do not occur in the excited state, the absence of a strong optical transition near 450 nm in the absorption spectrum taken together with the constant PL line width (Figure 2b) strongly suggest that radiative recombination cannot account for the ∼30 ps decay observed here.

Recently, Dohnalova and co-workers suggested an intrinsic origin to the blue band observed for alkyl-terminated Si NPs prepared via a wet chemical synthesis.[13] For these NPs, they report primarily blue PL and an absence of red emission, suggesting that the blue band is not related to hot exciton emission (a scenario in which one would expect to see blue and band-edge red PL). Following intense laser irradiation they observe an increase of red PL, which they attribute to sample oxidation. However, their results may also be interpreted in the context of our work as arising from changes in sample crystallinity. The wet chemical synthesis used in the study by Dohnalova et al. may not have provided sufficient energy to form c-Si, a covalently bonded material. Upon laser irradiation,

dx.doi.org/10.1021/ph500145p | ACS Photonics 2014, 1, 960−967

we suggest that sample annealing occurs, increasing the amount of crystalline material present and, consequently, the relative intensity of the red PL, which we and others attribute to indirect gap, band-edge recombination. Similarly, a recent study by Dasog and co-workers found that Si NPs synthesized at higher temperatures exhibited red, indirect gap photoluminescence, while Si NPs synthesized via more mild colloidal routes yielded rapid, blue photoluminescence.[37] These results, taken in conjunction with our presented data, lead us to the conclusion that high-energy PL is a result of emission arising from amorphous material. The persistence of amorphous material even in our most crystalline samples is supported by near-exact agreement between experimental Raman scattering spectra for c-Si NPs and theoretical Raman spectra calculated for crystalline core particles covered by a two-monolayer amorphous shell. The presence of amorphous material in the form of a persistent shell is supported by our observation of a disordered surface layer in TEM images as well as the presence of SiH_3 and SiH_2 on the NP surface (see Supporting Information).

In addition to the spectral similarities noted above for amorphous Si NPs and the blue feature observed in crystalline Si NPs, we find that PL dynamics for amorphous Si strongly resemble those found for the blue feature in crystalline Si. Indeed, regardless of sample size or crystallinity, we find the fastest PL decay observed to have a time constant of ~30 ps. This is depicted in Figure 4b, which shows the fitted time constant obtained for the fastest decay in the system for each sample considered in this study. The similarity and time scale of these dynamics suggests that in all cases, rapid PL decay is caused by the same (nonradiative) process. Furthermore, the longer component of the blue PL decay, for each power used, has a fitted time constant between 150 and 200 ps, very similar to the highly crystalline Si NPs studied in this work (Table 1). The rapid decay process we observe in completely amorphous (8 W) Si NPs is likely hole trapping in the strained regions of the amorphous network. This type of trapping was suggested in recent theoretical works by Lajoie et al.[38] and Wagner et al.[39] Given that a multitude of characterization methods (TEM, FTIR, Raman) indicate that highly crystalline particles still present an amorphous surface layer, we suggest that hole trapping processes occur in this thin amorphous shell.

Overall, we have identified and resolved, in the energy and time domains, a high energy (400−600 nm) band in the PL spectrum of plasma-synthesized, covalently functionalized Si NPs. Our findings constitute a comprehensive examination of the ultrafast dynamics of the 400-to-600 nm PL band previously attributed to both defect-related recombination and phononless PL in Si NPs. Whereas previous reports noted instrumentation-limited decay features, we examine these features with instruments having a response time adequate to resolve them. This new information allows us to resolve long-standing controversies regarding the fast PL band in quantum confined Si and conclusively attribute observed dynamics to a nonradiative decay process which we suggest is hole trapping in a persistent surface layer of amorphous Si. For the first time, we also examine the role of core crystallinity in PL. These results shed light on the origin of high energy PL in Si NPs and also provide an explanation for the observation of this PL in a wide variety of Si NP preparations, as they do not invoke surface chemistry or pseudodirect gap recombination. We expect that our work will stimulate future experimental and theoretical efforts regarding the role of lattice disorder in the optical properties of silicon nanomaterials. Furthermore, these findings present an opportunity for the systematic tailoring of absorption and emission spectra via core crystallinity, providing an additional degree of tunability to this technologically important class of materials.

METHODS

Nanocrystal Synthesis and Sample Preparation. The Si NPs studied here were fabricated by room-temperature plasma dissociation of SiH_4 using a previously described system.[40] A mixture of SiH_4/He (5/95% by volume) and argon was introduced into a quartz 13.56 MHz radio frequency (8−100 W) plasma reactor with 6.3 mm inner diameter and 9.5 mm outer diameter, at flow rates of 13 and 35−100 standard cubic centimeters per minute (sccm), respectively. Variation of the plasma power permits tunability of the NP crystallinity from highly amorphous to highly crystalline. Samples synthesized at powers of 80 W or above will be referred to as crystalline Si (c-Si). An additional H_2 flow (100 sccm) was injected at the afterglow region of the plasma to quench particle temperature and terminate dangling bond states.[28] NP size was controlled by particle synthesis pressure and examined by XRD. Indicated NP radii result from Scherrer analysis of such XRD diffraction peaks. The particles were collected on mesh filters and ultrasonicated to obtain a suspension in a mixture of 1-dodecene ligand and mesitylyene solvent with a ratio of 1:5 by volume. The suspension was transferred into a flask reactor and refluxed at 215 °C. Successful surface functionalization with dodecane was indicated by the change of cloudy suspension into clear solution. All steps were carried out in an inert environment.

Transient Photoluminescence Experiments. Alkyl-passivated Si NPs were suspended in octane and loaded into an airtight cuvette under a nitrogen atmosphere. The room-temperature NPs were photoexcited with 35 fs pulses from a 2 kHz amplified Ti-sapphire laser at 325 nm (3.8 eV). Excitation fluence sufficient to ensure single exciton dynamics ($N_{exc} \ll 1$) was utilized. PL photons were directed to a 150 mm spectrograph and single-photon-sensitive streak camera. Detector regions were binned vertically or horizontally to produce time-resolved spectra or spectrally resolved dynamics, respectively. It is important to note that the time resolution of a streak camera inherently depends on the observation window. Longer observation windows necessarily yield reduced temporal resolution, and vice versa. Therefore, dynamics which appear well-resolved by a streak camera utilizing a 120 ps observation window can appear instrumentally limited when examined using longer observation windows.

ASSOCIATED CONTENT

Supporting Information

Transmission electron microscopy images of silicon nanoparticles, FTIR spectra, details of molecular dynamics simulations, photoluminescence dynamics from 0−800 ps, and a detailed description of the fitting procedure used to determine relative amorphous content. This material is available free of charge via the Internet at http://pubs.acs.org.

AUTHOR INFORMATION

Corresponding Author

*E-mail: schaller@northwestern.edu.

Notes

The authors declare no competing financial interest.

■ ACKNOWLEDGMENTS

Use of the Center for Nanoscale Materials was supported by the U.S. Department of Energy, Office of Science, Office of Basic Energy Sciences, under Contract No. DE-AC02-06CH11357. J.Y., N.J.K. and U.R.K. were supported by the Center for Advanced Solar Photophysics, an Energy Frontier Research Center funded by the Department of Energy, Office of Basic Energy Sciences. D.C.H. acknowledges support from NSF Graduate Fellowship DGE-0824162. G.C.S. was supported by Grant DE-SC0004752 of the Office of Basic Energy Sciences.

■ REFERENCES

(1) Wilson, W. L.; Szajowski, P. F.; Brus, L. E. Quantum Confinement in Size-Selected, Surface-Oxidized Silicon Nanocrystals. *Science* **1993**, *262*, 1242−1244.
(2) Sykora, M.; Mangolini, L.; Schaller, R. D.; Kortshagen, U.; Jurbergs, D.; Klimov, V. I. Size-Dependent Intrinsic Radiative Decay Rates of Silicon Nanocrystals at Large Confinement Energies. *Phys. Rev. Lett.* **2008**, *100*, 067401.
(3) Jurbergs, D.; Rogojina, E.; Mangolini, L.; Kortshagen, U. Silicon Nanocrystals with Ensemble Quantum Yields Exceeding 60%. *Appl. Phys. Lett.* **2006**, *88*, 233116−3.
(4) Mangolini, L.; Jurbergs, D.; Rogojina, E.; Kortshagen, U. High Efficiency Photoluminescence from Silicon Nanocrystals Prepared by Plasma Synthesis and Organic Surface Passivation. *Physica Status Solidi C* **2006**, *3*, 3975−3978.
(5) de Boer, W. D. A. M.; Timmerman, D.; Dohnalova, K.; Yassievich, I. N.; Zhang, H.; Buma, W. J.; Gregorkiewicz, T. Red Spectral Shift and Enhanced Quantum Efficiency in Phonon-Free Photoluminescence from Silicon Nanocrystals. *Nat. Nano* **2010**, *5*, 878−884.
(6) English, D. S.; Pell, L. E.; Yu, Z.; Barbara, P. F.; Korgel, B. A. Size Tunable Visible Luminescence from Individual Organic Monolayer Stabilized Silicon Nanocrystal Quantum Dots. *Nano Lett.* **2002**, *2*, 681−685.
(7) Kůsová, K.; Cibulka, O.; Dohnalová, K.; Pelant, I.; Valenta, J.; Fučíková, A.; Žídek, K.; Lang, J.; Englich, J.; Matějka, P.; Štěpánek, P.; Bakardjieva, S. Brightly Luminescent Organically Capped Silicon Nanocrystals Fabricated at Room Temperature and Atmospheric Pressure. *ACS Nano* **2010**, *4*, 4495−4504.
(8) Groenewegen, V.; Kuntermann, V.; Haarer, D.; Kunz, M.; Kryschi, C. Excited-State Relaxation Dynamics of 3-Vinylthiophene-Terminated Silicon Quantum Dots. *J. Phys. Chem. C* **2010**, *114*, 11693−11698.
(9) Kanemitsu, Y. Luminescence Properties of Nanometer-Sized Si Crystallites: Core and Surface States. *Phys. Rev. B* **1994**, *49*, 16845−16848.
(10) Puzder, A.; Williamson, A. J.; Grossman, J. C.; Galli, G. Surface Chemistry of Silicon Nanoclusters. *Phys. Rev. Lett.* **2002**, *88*, 097401.
(11) Godefroo, S.; Hayne, M.; Jivanescu, M.; Stesmans, A.; Zacharias, M.; Lebedev, O. I.; Van Tendeloo, G.; Moshchalkov, V. V. Classification and Control of the Origin of Photoluminescence from Si Nanocrystals. *Nat. Nano* **2008**, *3*, 174−178.
(12) Žídek, K.; Pelant, I.; Trojánek, F.; Malý, P.; Gilliot, P.; Hönerlage, B.; Oberlé, J.; Šiller, L.; Little, R.; Horrocks, B. R. Ultrafast Stimulated Emission Due to Quasidirect Transitions in Silicon Nanocrystals. *Phys. Rev. B* **2011**, *84*, 085321.
(13) Dohnalova, K.; Poddubny, A. N.; Prokofiev, A. A.; de Boer, W. D. A. M.; Umesh, C. P.; Paulusse, J. M. J.; Zuilhof, H.; Gregorkiewicz, T. Surface Brightens up Si Quantum Dots: Direct Bandgap-Like Size-Tunable Emission. *Light Sci. Appl.* **2013**, *2*, e47.
(14) Allan, G.; Delerue, C.; Lannoo, M. Nature of Luminescent Surface States of Semiconductor Nanocrystallites. *Phys. Rev. Lett.* **1996**, *76*, 2961−2964.
(15) Hannah, D. C.; Yang, J.; Podsiadlo, P.; Chan, M. K. Y.; Demortière, A.; Gosztola, D. J.; Prakapenka, V. B.; Schatz, G. C.; Kortshagen, U.; Schaller, R. D. On the Origin of Photoluminescence in Silicon Nanocrystals: Pressure-Dependent Structural and Optical Studies. *Nano Lett.* **2012**, *12*, 4200−4205.
(16) Kovalev, D. Silicon Photonics: Moving into the Red. *Nat. Nano* **2010**, *5*, 827−828.
(17) Kovalev, D.; Polisski, G.; Ben, x; Chorin, M.; Diener, J.; Koch, F. The Temperature Dependence of the Absorption Coefficient of Porous Silicon. *J. Appl. Phys.* **1996**, *80*, 5978−5983.
(18) Kovalev, D.; Diener, J.; Heckler, H.; Polisski, G.; Künzner, N.; Koch, F. Optical Absorption Cross Sections of Si Nanocrystals. *Phys. Rev. B* **2000**, *61*, 4485−4487.
(19) Tsybeskov, L.; Vandyshev, J. V.; Fauchet, P. M. Blue Emission in Porous Silicon: Oxygen-Related Photoluminescence. *Phys. Rev. B* **1994**, *49*, 7821−7824.
(20) Valenta, J.; Fucikova, A.; Pelant, I.; Kůsová, K.; Dohnalová, K.; Aleknavičius, A.; Cibulka, O.; Fojtík, A.; Kada, G. On the origin of the fast photoluminescence band in small silicon nanoparticles. *New J. Phys.* **2008**, *10*, 073022.
(21) Yang, C.-S.; Bley, R. A.; Kauzlarich, S. M.; Lee, H. W. H.; Delgado, G. R. Synthesis of Alkyl-Terminated Silicon Nanoclusters by a Solution Route. *J. Am. Chem. Soc.* **1999**, *121*, 5191−5195.
(22) Holmes, J. D.; Ziegler, K. J.; Doty, R. C.; Pell, L. E.; Johnston, K. P.; Korgel, B. A. Highly Luminescent Silicon Nanocrystals with Discrete Optical Transitions. *J. Am. Chem. Soc.* **2001**, *123*, 3743−3748.
(23) Pietryga, J. M.; Zhuravlev, K. K.; Whitehead, M.; Klimov, V. I.; Schaller, R. D. Evidence for Barrierless Auger Recombination in PbSe Nanocrystals: A Pressure-Dependent Study of Transient Optical Absorption. *Phys. Rev. Lett.* **2008**, *101*, 217401.
(24) Nirmal, M.; Norris, D. J.; Kuno, M.; Bawendi, M. G.; Efros, A. L.; Rosen, M. Observation of the "Dark Exciton" in CdSe Quantum Dots. *Phys. Rev. Lett.* **1995**, *75*, 3728−3731.
(25) Klimov, V. I.; McBranch, D. W. Femtosecond 1P-to-1S Electron Relaxation in Strongly Confined Semiconductor Nanocrystals. *Phys. Rev. Lett.* **1998**, *80*, 4028−4031.
(26) Schaller, R. D.; Pietryga, J. M.; Goupalov, S. V.; Petruska, M. A.; Ivanov, S. A.; Klimov, V. I. Breaking the Phonon Bottleneck in Semiconductor Nanocrystals via Multiphonon Emission Induced by Intrinsic Nonadiabatic Interactions. *Phys. Rev. Lett.* **2005**, *95*, 196401.
(27) Anthony, R.; Kortshagen, U. Photoluminescence Quantum Yields of Amorphous and Crystalline Silicon Nanoparticles. *Phys. Rev. B* **2009**, *80*, 115407.
(28) Anthony, R. J.; Rowe, D. J.; Stein, M.; Yang, J.; Kortshagen, U. Routes to Achieving High Quantum Yield Luminescence from Gas-Phase-Produced Silicon Nanocrystals. *Adv. Funct. Mater.* **2011**, *21*, 4042−4046.
(29) Pankove, J. I.; Carlson, D. E. Photoluminescence of Hydrogenated Amorphous Silicon. *Appl. Phys. Lett.* **1977**, *31*, 450−451.
(30) Wang, Y. Q.; Wang, Y. G.; Cao, L.; Cao, Z. X. High-Efficiency Visible Photoluminescence from Amorphous Silicon Nanoparticles Embedded in Silicon Nitride. *Appl. Phys. Lett.* **2003**, *83*, 3474−3476.
(31) Wehrspohn, R. B.; Chazalviel, J. N.; Ozanam, F.; Solomon, I. Electrochemistry and Photoluminescence of Porous Amorphous Silicon. *Thin Solid Films* **1997**, *297*, 5−8.
(32) Duan, Y.; Kong, J. F.; Shen, W. Z. Raman Investigation of Silicon Nanocrystals: Quantum Confinement and Laser-Induced Thermal Effects. *J. Raman Spectrosc.* **2012**, *43*, 756−760.
(33) Ristić, D.; Ivanda, M.; Furić, K. Application of the Phonon Confinement Model on the Optical Phonon Mode of Silicon Nanoparticles. *J. Mol. Struct.* **2009**, *924*−*926*, 291−293.
(34) Panthani, M. G.; Hessel, C. M.; Reid, D.; Casillas, G.; José-Yacamán, M.; Korgel, B. A. Graphene-Supported High-Resolution TEM and STEM Imaging of Silicon Nanocrystals and their Capping Ligands. *J. Phys. Chem. C* **2012**, *116*, 22463−22468.

(35) Smit, C.; van Swaaij, R. A. C. M. M.; Donker, H.; Petit, A. M. H. N.; Kessels, W. M. M.; van de Sanden, M. C. M. Determining the Material Structure of Microcrystalline Silicon from Raman Spectra. *J. Appl. Phys.* **2003**, *94*, 3582−3588.
(36) Gresback, R.; Hue, R.; Gladfelter, W.; Kortshagen, U. Combined Plasma Gas-Phase Synthesis and Colloidal Processing of InP/ZnS Core/Shell Nanocrystals. *Nanoscale Res. Lett.* **2011**, *6*, 68.
(37) Dasog, M.; Yang, Z.; Regli, S.; Atkins, T. M.; Faramus, A.; Singh, M. P.; Muthuswamy, E.; Kauzlarich, S. M.; Tilley, R. D.; Veinot, J. G. C. Chemical Insight into the Origin of Red and Blue Photoluminescence Arising from Freestanding Silicon Nanocrystals. *ACS Nano* **2013**, *7*, 2676−2685.
(38) Lajoie, T. W.; Ramirez, J. J.; Kilin, D. S.; Micha, D. A. Optical Properties of Amorphous and Crystalline Silicon Surfaces Functionalized with Agn Adsorbates. *Int. J. Quantum Chem.* **2010**, *110*, 3005−3014.
(39) Wagner, L. K.; Grossman, J. C. Microscopic Description of Light Induced Defects in Amorphous Silicon Solar Cells. *Phys. Rev. Lett.* **2008**, *101*, 265501.
(40) Mangolini, L.; Kortshagen, U. Plasma-Assisted Synthesis of Silicon Nanocrystal Inks. *Adv. Mater.* **2007**, *19*, 2513−2519.